

Dalitz Plot Analysis of $B^\pm \rightarrow \pi^\pm \pi^\pm \pi^\mp$ Decays

B. Aubert,¹ Y. Karyotakis,¹ J. P. Lees,¹ V. Poireau,¹ E. Prencipe,¹ X. Prudent,¹ V. Tisserand,¹ J. Garra Tico,²
E. Grauges,² L. Lopez^{ab,3}, A. Palano^{ab,3}, M. Pappagallo^{ab,3}, G. Eigen,⁴ B. Stugu,⁴ L. Sun,⁴ M. Battaglia,⁵
D. N. Brown,⁵ L. T. Kerth,⁵ Yu. G. Kolomensky,⁵ G. Lynch,⁵ I. L. Osipenkov,⁵ K. Tackmann,⁵ T. Tanabe,⁵
C. M. Hawkes,⁶ N. Soni,⁶ A. T. Watson,⁶ H. Koch,⁷ T. Schroeder,⁷ D. J. Asgeirsson,⁸ B. G. Fulsom,⁸ C. Hearty,⁸
T. S. Mattison,⁸ J. A. McKenna,⁸ M. Barrett,⁹ A. Khan,⁹ A. Randle-Conde,⁹ V. E. Blinov,¹⁰ A. D. Bukin,^{10,*}
A. R. Buzykaev,¹⁰ V. P. Druzhinin,¹⁰ V. B. Golubev,¹⁰ A. P. Onuchin,¹⁰ S. I. Serednyakov,¹⁰ Yu. I. Skovpen,¹⁰
E. P. Solodov,¹⁰ K. Yu. Todyshev,¹⁰ M. Bondioli,¹¹ S. Curry,¹¹ I. Eschrich,¹¹ D. Kirkby,¹¹ A. J. Lankford,¹¹
P. Lund,¹¹ M. Mandelkern,¹¹ E. C. Martin,¹¹ D. P. Stoker,¹¹ S. Abachi,¹² C. Buchanan,¹² H. Atmacan,¹³
J. W. Gary,¹³ F. Liu,¹³ O. Long,¹³ G. M. Vitug,¹³ Z. Yasin,¹³ L. Zhang,¹³ V. Sharma,¹⁴ C. Campagnari,¹⁵
T. M. Hong,¹⁵ D. Kovalskyi,¹⁵ M. A. Mazur,¹⁵ J. D. Richman,¹⁵ T. W. Beck,¹⁶ A. M. Eisner,¹⁶ C. A. Heusch,¹⁶
J. Kroseberg,¹⁶ W. S. Lockman,¹⁶ A. J. Martinez,¹⁶ T. Schalk,¹⁶ B. A. Schumm,¹⁶ A. Seiden,¹⁶ L. O. Winstrom,¹⁶
C. H. Cheng,¹⁷ D. A. Doll,¹⁷ B. Echenard,¹⁷ F. Fang,¹⁷ D. G. Hitlin,¹⁷ I. Narsky,¹⁷ T. Piatenko,¹⁷ F. C. Porter,¹⁷
R. Andreassen,¹⁸ G. Mancinelli,¹⁸ B. T. Meadows,¹⁸ K. Mishra,¹⁸ M. D. Sokoloff,¹⁸ P. C. Bloom,¹⁹ W. T. Ford,¹⁹
A. Gaz,¹⁹ J. F. Hirschauer,¹⁹ M. Nagel,¹⁹ U. Nauenberg,¹⁹ J. G. Smith,¹⁹ S. R. Wagner,¹⁹ R. Ayad,^{20,†}
A. Soffer,^{20,‡} W. H. Toki,²⁰ R. J. Wilson,²⁰ E. Feltresi,²¹ A. Hauke,²¹ H. Jasper,²¹ M. Karbach,²¹ J. Merkel,²¹
A. Petzold,²¹ B. Spaan,²¹ K. Wacker,²¹ M. J. Kobel,²² R. Nogowski,²² K. R. Schubert,²² R. Schwierz,²² A. Volk,²²
D. Bernard,²³ G. R. Bonneaud,²³ E. Latour,²³ M. Verderi,²³ P. J. Clark,²⁴ S. Playfer,²⁴ J. E. Watson,²⁴
M. Andreotti^{ab,25}, D. Bettoni^{a,25}, C. Bozzi^{a,25}, R. Calabrese^{ab,25}, A. Cecchi^{ab,25}, G. Cibinetto^{ab,25}, P. Franchini^{ab,25},
E. Luppi^{ab,25}, M. Negrini^{ab,25}, A. Petrella^{ab,25}, L. Piemontese^{a,25}, V. Santoro^{ab,25}, R. Baldini-Ferrolli,²⁶
A. Calcaterra,²⁶ R. de Sangro,²⁶ G. Finocchiaro,²⁶ S. Pacetti,²⁶ P. Patteri,²⁶ I. M. Peruzzi,^{26,§} M. Piccolo,²⁶
M. Rama,²⁶ A. Zallo,²⁶ R. Contri^{ab,27}, E. Guido,²⁷ M. Lo Vetere^{ab,27}, M. R. Monge^{ab,27}, S. Passaggio^{a,27},
C. Patrignani^{ab,27}, E. Robutti^{a,27}, S. Tosi^{ab,27}, K. S. Chaisanguanthum,²⁸ M. Morii,²⁸ A. Adametz,²⁹ J. Marks,²⁹
S. Schenk,²⁹ U. Uwer,²⁹ F. U. Bernlochner,³⁰ V. Klose,³⁰ H. M. Lacker,³⁰ D. J. Bard,³¹ P. D. Dauncey,³¹
M. Tibbetts,³¹ P. K. Behera,³² X. Chai,³² M. J. Charles,³² U. Mallik,³² J. Cochran,³³ H. B. Crawley,³³ L. Dong,³³
W. T. Meyer,³³ S. Prell,³³ E. I. Rosenberg,³³ A. E. Rubin,³³ Y. Y. Gao,³⁴ A. V. Gritsan,³⁴ Z. J. Guo,³⁴
N. Arnaud,³⁵ J. Béquilleux,³⁵ A. D’Orazio,³⁵ M. Davier,³⁵ J. Firmino da Costa,³⁵ G. Grosdidier,³⁵ F. Le Diberder,³⁵
V. Lepeltier,³⁵ A. M. Lutz,³⁵ S. Pruvot,³⁵ P. Roudeau,³⁵ M. H. Schune,³⁵ J. Serrano,³⁵ V. Sordini,^{35,¶} A. Stocchi,³⁵
G. Wormser,³⁵ D. J. Lange,³⁶ D. M. Wright,³⁶ I. Bingham,³⁷ J. P. Burke,³⁷ C. A. Chavez,³⁷ J. R. Fry,³⁷
E. Gabathuler,³⁷ R. Gamet,³⁷ D. E. Hutchcroft,³⁷ D. J. Payne,³⁷ C. Touramanis,³⁷ A. J. Bevan,³⁸ C. K. Clarke,³⁸
F. Di Lodovico,³⁸ R. Sacco,³⁸ M. Sigamani,³⁸ G. Cowan,³⁹ S. Paramesvaran,³⁹ A. C. Wren,³⁹ D. N. Brown,⁴⁰
C. L. Davis,⁴⁰ A. G. Denig,⁴¹ M. Fritsch,⁴¹ W. Gradl,⁴¹ A. Hafner,⁴¹ K. E. Alwyn,⁴² D. Bailey,⁴² R. J. Barlow,⁴²
G. Jackson,⁴² G. D. Lafferty,⁴² T. J. West,⁴² J. I. Yi,⁴² J. Anderson,⁴³ C. Chen,⁴³ A. Jawahery,⁴³ D. A. Roberts,⁴³
G. Simi,⁴³ J. M. Tuggle,⁴³ C. Dallapiccola,⁴⁴ E. Salvati,⁴⁴ S. Saremi,⁴⁴ R. Cowan,⁴⁵ D. Dujmic,⁴⁵ P. H. Fisher,⁴⁵
S. W. Henderson,⁴⁵ G. Sciolla,⁴⁵ M. Spitznagel,⁴⁵ R. K. Yamamoto,⁴⁵ M. Zhao,⁴⁵ P. M. Patel,⁴⁶ S. H. Robertson,⁴⁶
M. Schram,⁴⁶ A. Lazzaro^{ab,47}, V. Lombardo^{a,47}, F. Palombo^{ab,47}, S. Stracka,⁴⁷ J. M. Bauer,⁴⁸ L. Cremaldi,⁴⁸
R. Godang,^{48,**} R. Kroeger,⁴⁸ D. J. Summers,⁴⁸ H. W. Zhao,⁴⁸ M. Simard,⁴⁹ P. Taras,⁴⁹ H. Nicholson,⁵⁰
G. De Nardo^{ab,51}, L. Lista^{a,51}, D. Monorchio^{ab,51}, G. Onorato^{ab,51}, C. Sciacca^{ab,51}, G. Raven,⁵² H. L. Snoek,⁵²
C. P. Jessop,⁵³ K. J. Knoepfel,⁵³ J. M. LoSecco,⁵³ W. F. Wang,⁵³ L. A. Corwin,⁵⁴ K. Honscheid,⁵⁴ H. Kagan,⁵⁴
R. Kass,⁵⁴ J. P. Morris,⁵⁴ A. M. Rahimi,⁵⁴ J. J. Regensburger,⁵⁴ S. J. Sekula,⁵⁴ Q. K. Wong,⁵⁴ N. L. Blount,⁵⁵
J. Brau,⁵⁵ R. Frey,⁵⁵ O. Igonkina,⁵⁵ J. A. Kolb,⁵⁵ M. Lu,⁵⁵ R. Rahmat,⁵⁵ N. B. Sinev,⁵⁵ D. Strom,⁵⁵ J. Strube,⁵⁵
E. Torrence,⁵⁵ G. Castelli^{ab,56}, N. Gagliardi^{ab,56}, M. Margoni^{ab,56}, M. Morandin^{a,56}, M. Posocco^{a,56}, M. Rotondo^{a,56},
F. Simonetto^{ab,56}, R. Stroili^{ab,56}, C. Voci^{ab,56}, P. del Amo Sanchez,⁵⁷ E. Ben-Haim,⁵⁷ H. Briand,⁵⁷ J. Chauveau,⁵⁷
O. Hamon,⁵⁷ Ph. Leruste,⁵⁷ J. Ocariz,⁵⁷ A. Perez,⁵⁷ J. Prendki,⁵⁷ S. Sitt,⁵⁷ L. Gladney,⁵⁸ M. Biasini^{ab,59},
E. Manoni^{ab,59}, C. Angelini^{ab,60}, G. Batignani^{ab,60}, S. Bettarini^{ab,60}, G. Calderini^{ab,60,††}, M. Carpinelli^{ab,60,‡‡},
A. Cervelli^{ab,60}, F. Forti^{ab,60}, M. A. Giorgi^{ab,60}, A. Lusiani^{ac,60}, G. Marchiori^{ab,60}, M. Morganti^{ab,60}, N. Neri^{ab,60},
E. Paoloni^{ab,60}, G. Rizzo^{ab,60}, J. J. Walsh^{a,60}, D. Lopes Pegna,⁶¹ C. Lu,⁶¹ J. Olsen,⁶¹ A. J. S. Smith,⁶¹

A. V. Telnov,⁶¹ F. Anulli^{a,62} E. Baracchini^{ab,62} G. Cavoto^{a,62} R. Faccini^{ab,62} F. Ferrarotto^{a,62} F. Ferroni^{ab,62} M. Gaspero^{ab,62} P. D. Jackson^{a,62} L. Li Gioi^{a,62} M. A. Mazzoni^{a,62} S. Morganti^{a,62} G. Piredda^{a,62} F. Renga^{ab,62} C. Voena^{a,62} M. Ebert,⁶³ T. Hartmann,⁶³ H. Schröder,⁶³ R. Waldi,⁶³ T. Adye,⁶⁴ B. Franek,⁶⁴ E. O. Olaiya,⁶⁴ F. F. Wilson,⁶⁴ S. Emery,⁶⁵ L. Esteve,⁶⁵ G. Hamel de Monchenault,⁶⁵ W. Kozanecki,⁶⁵ G. Vasseur,⁶⁵ Ch. Yèche,⁶⁵ M. Zito,⁶⁵ X. R. Chen,⁶⁶ H. Liu,⁶⁶ W. Park,⁶⁶ M. V. Purohit,⁶⁶ R. M. White,⁶⁶ J. R. Wilson,⁶⁶ M. T. Allen,⁶⁷ D. Aston,⁶⁷ R. Bartoldus,⁶⁷ J. F. Benitez,⁶⁷ R. Cenci,⁶⁷ J. P. Coleman,⁶⁷ M. R. Convery,⁶⁷ J. C. Dingfelder,⁶⁷ J. Dorfan,⁶⁷ G. P. Dubois-Felsmann,⁶⁷ W. Dunwoodie,⁶⁷ R. C. Field,⁶⁷ A. M. Gabareen,⁶⁷ M. T. Graham,⁶⁷ P. Grenier,⁶⁷ C. Hast,⁶⁷ W. R. Innes,⁶⁷ J. Kaminski,⁶⁷ M. H. Kelsey,⁶⁷ H. Kim,⁶⁷ P. Kim,⁶⁷ M. L. Kocian,⁶⁷ D. W. G. S. Leith,⁶⁷ S. Li,⁶⁷ B. Lindquist,⁶⁷ S. Luitz,⁶⁷ V. Luth,⁶⁷ H. L. Lynch,⁶⁷ D. B. MacFarlane,⁶⁷ H. Marsiske,⁶⁷ R. Messner,^{67,*} D. R. Muller,⁶⁷ H. Neal,⁶⁷ S. Nelson,⁶⁷ C. P. O'Grady,⁶⁷ I. Ofte,⁶⁷ M. Perl,⁶⁷ B. N. Ratcliff,⁶⁷ A. Roodman,⁶⁷ A. A. Salnikov,⁶⁷ R. H. Schindler,⁶⁷ J. Schwiening,⁶⁷ A. Snyder,⁶⁷ D. Su,⁶⁷ M. K. Sullivan,⁶⁷ K. Suzuki,⁶⁷ S. K. Swain,⁶⁷ J. M. Thompson,⁶⁷ J. Va'vra,⁶⁷ A. P. Wagner,⁶⁷ M. Weaver,⁶⁷ C. A. West,⁶⁷ W. J. Wisniewski,⁶⁷ M. Wittgen,⁶⁷ D. H. Wright,⁶⁷ H. W. Wulsin,⁶⁷ A. K. Yarritu,⁶⁷ K. Yi,⁶⁷ C. C. Young,⁶⁷ V. Ziegler,⁶⁷ P. R. Burchat,⁶⁸ A. J. Edwards,⁶⁸ T. S. Miyashita,⁶⁸ S. Ahmed,⁶⁹ M. S. Alam,⁶⁹ J. A. Ernst,⁶⁹ B. Pan,⁶⁹ M. A. Saeed,⁶⁹ S. B. Zain,⁶⁹ S. M. Spanier,⁷⁰ B. J. Wogslund,⁷⁰ R. Eckmann,⁷¹ J. L. Ritchie,⁷¹ A. M. Ruland,⁷¹ C. J. Schilling,⁷¹ R. F. Schwitters,⁷¹ B. W. Drummond,⁷² J. M. Izen,⁷² X. C. Lou,⁷² F. Bianchi^{ab,73} D. Gamba^{ab,73} M. Pelliccioni^{ab,73} M. Bomben^{ab,74} L. Bosisio^{ab,74} C. Cartaro^{ab,74} G. Della Ricca^{ab,74} L. Lanceri^{ab,74} L. Vitale^{ab,74} V. Azzolini,⁷⁵ N. Lopez-March,⁷⁵ F. Martinez-Vidal,⁷⁵ D. A. Milanes,⁷⁵ A. Oyanguren,⁷⁵ J. Albert,⁷⁶ Sw. Banerjee,⁷⁶ B. Bhuyan,⁷⁶ H. H. F. Choi,⁷⁶ K. Hamano,⁷⁶ G. J. King,⁷⁶ R. Kowalewski,⁷⁶ M. J. Lewczuk,⁷⁶ I. M. Nugent,⁷⁶ J. M. Roney,⁷⁶ R. J. Sobie,⁷⁶ J. J. Back,⁷⁷ T. J. Gershon,⁷⁷ P. F. Harrison,⁷⁷ J. Ilic,⁷⁷ T. E. Latham,⁷⁷ G. B. Mohanty,⁷⁷ E. M. T. Puccio,⁷⁷ H. R. Band,⁷⁸ X. Chen,⁷⁸ S. Dasu,⁷⁸ K. T. Flood,⁷⁸ Y. Pan,⁷⁸ R. Prepost,⁷⁸ C. O. Vuosalo,⁷⁸ and S. L. Wu⁷⁸

(The BABAR Collaboration)

¹Laboratoire d'Annecy-le-Vieux de Physique des Particules (LAPP),
Universit  de Savoie, CNRS/IN2P3, F-74941 Annecy-Le-Vieux, France

²Universitat de Barcelona, Facultat de Fisica, Departament ECM, E-08028 Barcelona, Spain

³INFN Sezione di Bari^a; Dipartimento di Fisica, Universit  di Bari^b, I-70126 Bari, Italy

⁴University of Bergen, Institute of Physics, N-5007 Bergen, Norway

⁵Lawrence Berkeley National Laboratory and University of California, Berkeley, California 94720, USA

⁶University of Birmingham, Birmingham, B15 2TT, United Kingdom

⁷Ruhr Universit  Bochum, Institut f r Experimentalphysik 1, D-44780 Bochum, Germany

⁸University of British Columbia, Vancouver, British Columbia, Canada V6T 1Z1

⁹Brunel University, Uxbridge, Middlesex UB8 3PH, United Kingdom

¹⁰Budker Institute of Nuclear Physics, Novosibirsk 630090, Russia

¹¹University of California at Irvine, Irvine, California 92697, USA

¹²University of California at Los Angeles, Los Angeles, California 90024, USA

¹³University of California at Riverside, Riverside, California 92521, USA

¹⁴University of California at San Diego, La Jolla, California 92093, USA

¹⁵University of California at Santa Barbara, Santa Barbara, California 93106, USA

¹⁶University of California at Santa Cruz, Institute for Particle Physics, Santa Cruz, California 95064, USA

¹⁷California Institute of Technology, Pasadena, California 91125, USA

¹⁸University of Cincinnati, Cincinnati, Ohio 45221, USA

¹⁹University of Colorado, Boulder, Colorado 80309, USA

²⁰Colorado State University, Fort Collins, Colorado 80523, USA

²¹Technische Universit  Dortmund, Fakult t Physik, D-44221 Dortmund, Germany

²²Technische Universit  Dresden, Institut f r Kern- und Teilchenphysik, D-01062 Dresden, Germany

²³Laboratoire Leprince-Ringuet, CNRS/IN2P3, Ecole Polytechnique, F-91128 Palaiseau, France

²⁴University of Edinburgh, Edinburgh EH9 3JZ, United Kingdom

²⁵INFN Sezione di Ferrara^a; Dipartimento di Fisica, Universit  di Ferrara^b, I-44100 Ferrara, Italy

²⁶INFN Laboratori Nazionali di Frascati, I-00044 Frascati, Italy

²⁷INFN Sezione di Genova^a; Dipartimento di Fisica, Universit  di Genova^b, I-16146 Genova, Italy

²⁸Harvard University, Cambridge, Massachusetts 02138, USA

²⁹Universit  Heidelberg, Physikalisches Institut, Philosophenweg 12, D-69120 Heidelberg, Germany

³⁰Humboldt-Universit  zu Berlin, Institut f r Physik, Newtonstr. 15, D-12489 Berlin, Germany

³¹Imperial College London, London, SW7 2AZ, United Kingdom

³²University of Iowa, Iowa City, Iowa 52242, USA

³³Iowa State University, Ames, Iowa 50011-3160, USA

³⁴Johns Hopkins University, Baltimore, Maryland 21218, USA

- ³⁵Laboratoire de l'Accélérateur Linéaire, IN2P3/CNRS et Université Paris-Sud 11,
Centre Scientifique d'Orsay, B. P. 34, F-91898 Orsay Cedex, France
- ³⁶Lawrence Livermore National Laboratory, Livermore, California 94550, USA
- ³⁷University of Liverpool, Liverpool L69 7ZE, United Kingdom
- ³⁸Queen Mary, University of London, London, E1 4NS, United Kingdom
- ³⁹University of London, Royal Holloway and Bedford New College, Egham, Surrey TW20 0EX, United Kingdom
- ⁴⁰University of Louisville, Louisville, Kentucky 40292, USA
- ⁴¹Johannes Gutenberg-Universität Mainz, Institut für Kernphysik, D-55099 Mainz, Germany
- ⁴²University of Manchester, Manchester M13 9PL, United Kingdom
- ⁴³University of Maryland, College Park, Maryland 20742, USA
- ⁴⁴University of Massachusetts, Amherst, Massachusetts 01003, USA
- ⁴⁵Massachusetts Institute of Technology, Laboratory for Nuclear Science, Cambridge, Massachusetts 02139, USA
- ⁴⁶McGill University, Montréal, Québec, Canada H3A 2T8
- ⁴⁷INFN Sezione di Milano^a; Dipartimento di Fisica, Università di Milano^b, I-20133 Milano, Italy
- ⁴⁸University of Mississippi, University, Mississippi 38677, USA
- ⁴⁹Université de Montréal, Physique des Particules, Montréal, Québec, Canada H3C 3J7
- ⁵⁰Mount Holyoke College, South Hadley, Massachusetts 01075, USA
- ⁵¹INFN Sezione di Napoli^a; Dipartimento di Scienze Fisiche,
Università di Napoli Federico II^b, I-80126 Napoli, Italy
- ⁵²NIKHEF, National Institute for Nuclear Physics and High Energy Physics, NL-1009 DB Amsterdam, The Netherlands
- ⁵³University of Notre Dame, Notre Dame, Indiana 46556, USA
- ⁵⁴Ohio State University, Columbus, Ohio 43210, USA
- ⁵⁵University of Oregon, Eugene, Oregon 97403, USA
- ⁵⁶INFN Sezione di Padova^a; Dipartimento di Fisica, Università di Padova^b, I-35131 Padova, Italy
- ⁵⁷Laboratoire de Physique Nucléaire et de Hautes Energies,
IN2P3/CNRS, Université Pierre et Marie Curie-Paris6,
Université Denis Diderot-Paris7, F-75252 Paris, France
- ⁵⁸University of Pennsylvania, Philadelphia, Pennsylvania 19104, USA
- ⁵⁹INFN Sezione di Perugia^a; Dipartimento di Fisica, Università di Perugia^b, I-06100 Perugia, Italy
- ⁶⁰INFN Sezione di Pisa^a; Dipartimento di Fisica,
Università di Pisa^b; Scuola Normale Superiore di Pisa^c, I-56127 Pisa, Italy
- ⁶¹Princeton University, Princeton, New Jersey 08544, USA
- ⁶²INFN Sezione di Roma^a; Dipartimento di Fisica,
Università di Roma La Sapienza^b, I-00185 Roma, Italy
- ⁶³Universität Rostock, D-18051 Rostock, Germany
- ⁶⁴Rutherford Appleton Laboratory, Chilton, Didcot, Oxon, OX11 0QX, United Kingdom
- ⁶⁵CEA, Irfu, SPP, Centre de Saclay, F-91191 Gif-sur-Yvette, France
- ⁶⁶University of South Carolina, Columbia, South Carolina 29208, USA
- ⁶⁷SLAC National Accelerator Laboratory, Stanford, California 94309, USA
- ⁶⁸Stanford University, Stanford, California 94305-4060, USA
- ⁶⁹State University of New York, Albany, New York 12222, USA
- ⁷⁰University of Tennessee, Knoxville, Tennessee 37996, USA
- ⁷¹University of Texas at Austin, Austin, Texas 78712, USA
- ⁷²University of Texas at Dallas, Richardson, Texas 75083, USA
- ⁷³INFN Sezione di Torino^a; Dipartimento di Fisica Sperimentale, Università di Torino^b, I-10125 Torino, Italy
- ⁷⁴INFN Sezione di Trieste^a; Dipartimento di Fisica, Università di Trieste^b, I-34127 Trieste, Italy
- ⁷⁵IFIC, Universitat de Valencia-CSIC, E-46071 Valencia, Spain
- ⁷⁶University of Victoria, Victoria, British Columbia, Canada V8W 3P6
- ⁷⁷Department of Physics, University of Warwick, Coventry CV4 7AL, United Kingdom
- ⁷⁸University of Wisconsin, Madison, Wisconsin 53706, USA

(Dated: October 22, 2018)

We present a Dalitz plot analysis of charmless B^\pm decays to the final state $\pi^\pm\pi^\pm\pi^\mp$ using a sample of $(465 \pm 5) \times 10^6$ $B\bar{B}$ pairs collected by the BABAR experiment at $\sqrt{s} = 10.58$ GeV. We measure the branching fractions $\mathcal{B}(B^\pm \rightarrow \pi^\pm\pi^\pm\pi^\mp) = (15.2 \pm 0.6 \pm 1.2 \pm 0.4) \times 10^{-6}$, $\mathcal{B}(B^\pm \rightarrow \rho^0(770)\pi^\pm) = (8.1 \pm 0.7 \pm 1.2^{+0.4}_{-1.1}) \times 10^{-6}$, $\mathcal{B}(B^\pm \rightarrow f_2(1270)\pi^\pm) = (1.57 \pm 0.42 \pm 0.16^{+0.53}_{-0.19}) \times 10^{-6}$, and $\mathcal{B}(B^\pm \rightarrow \pi^\pm\pi^\pm\pi^\mp \text{ nonresonant}) = (5.3 \pm 0.7 \pm 0.6^{+1.1}_{-0.5}) \times 10^{-6}$, where the uncertainties are statistical, systematic, and model-dependent, respectively. Measurements of branching fractions for the modes $B^\pm \rightarrow \rho^0(1450)\pi^\pm$ and $B^\pm \rightarrow f_0(1370)\pi^\pm$ are also presented. We observe no significant direct CP asymmetries for the above modes, and there is no evidence for the decays $B^\pm \rightarrow f_0(980)\pi^\pm$, $B^\pm \rightarrow \chi_{c0}\pi^\pm$, or $B^\pm \rightarrow \chi_{c2}\pi^\pm$.

PACS numbers: 13.25.Hw, 12.15.Hh, 11.30.Er

INTRODUCTION

Decays of B mesons to three-body charmless final states probe the properties of the weak interaction through their dependence on the complex quark couplings described in the Cabibbo-Kobayashi-Maskawa (CKM) matrix [1, 2]. Furthermore, these decays test dynamical models for hadronic B decays.

One can measure direct CP asymmetries and constrain magnitudes and phases of the CKM matrix elements using individual channels that appear as intermediate resonances in the $B^\pm \rightarrow \pi^\pm \pi^\pm \pi^\mp$ decay. For example, the CKM angle γ could be extracted from the interference between the decay $B^\pm \rightarrow \chi_{c0} \pi^\pm$, which has no CP -violating phase (in the standard parametrization), and other modes such as $B^\pm \rightarrow \rho^0(770) \pi^\pm$ [3, 4, 5, 6, 7, 8].

Studies of $B^\pm \rightarrow \pi^\pm \pi^\pm \pi^\mp$ can also be useful for a precise measurement of the CKM angle α . A theoretically clean determination of this angle can be obtained from the decay-time dependence of the interference between $B^0 \rightarrow \rho^+ \pi^-$, $B^0 \rightarrow \rho^- \pi^+$, and $B^0 \rightarrow \rho^0 \pi^0$ via the analysis of the Dalitz plot for $B^0 \rightarrow \pi^+ \pi^- \pi^0$ decays [9] (recently implemented by *BABAR* [10] and *Belle* [11, 12]). Charged B decays offer a large statistics sample with which to determine additional resonant or nonresonant contributions to the three-pion Dalitz plot that can affect the measurement of α . For example, the Dalitz plot analysis of $B^\pm \rightarrow \pi^\pm \pi^\pm \pi^\mp$ allows one to check for effects from $B^\pm \rightarrow \omega(782) \pi^\pm$, that could cause large direct CP violation due to ρ - ω mixing [13]. It is particularly important to limit the possible effects of broad scalar structures [including the so-called $f_0(600)$ or σ] and nonresonant contributions [14, 15, 16, 17, 18, 19].

Furthermore, a number of unexplained structures have been observed in charmless B decays to $K\pi\pi$ [20, 21, 22, 23, 24, 25], $KK\pi$ [26, 27], and KKK [23, 28, 29] final states. Verifying the presence of these structures in $B^\pm \rightarrow \pi^\pm \pi^\pm \pi^\mp$ decays would help to determine their nature and involvement in hadronic B decays.

In this paper we present an amplitude analysis of $B^\pm \rightarrow \pi^\pm \pi^\pm \pi^\mp$ decays based on a 424 fb^{-1} data sample containing $(465 \pm 5) \times 10^6$ $B\bar{B}$ pairs ($N_{B\bar{B}}$). The data were collected with the *BABAR* detector [30] at the PEP-II asymmetric-energy e^+e^- storage rings [31] operating at the $\Upsilon(4S)$ resonance with center-of-mass (CM) energy of $\sqrt{s} = 10.58 \text{ GeV}$. An additional total integrated luminosity of 44 fb^{-1} was recorded 40 MeV below the $\Upsilon(4S)$ resonance (“off-peak” data) and was used to study backgrounds. Compared to our previous publication [32], in addition to doubling the data sample we have included several improvements in reconstruction algorithms that enhance the signal efficiency, made numerous modifications to the analysis to increase the sensitivity to direct CP violation effects (for example, by including more discriminating variables in the maximum likelihood fit), and

improved our model of the Dalitz plot structure.

The remainder of the paper is organized as follows: Sec. II describes the amplitude analysis formalism, Secs. III and IV give details about the selection of signal B decays and how backgrounds are considered, Sec. V presents the results from the likelihood fit, Sec. VI gives an account of the various sources of systematic uncertainties, while Sec. VII summarizes the results.

AMPLITUDE ANALYSIS FORMALISM

A number of intermediate states contribute to the decay $B^\pm \rightarrow \pi^\pm \pi^\pm \pi^\mp$. We determine their contributions with a maximum likelihood fit to the distribution of events in the Dalitz plot. This procedure has been described in detail in our previous publications [20, 21, 32].

The $B^\pm \rightarrow \pi^\pm \pi^\pm \pi^\mp$ decay contains two same-sign pions in the final state. We distinguish these particles according to the invariant mass they make when combined with the oppositely charged pion, and draw the Dalitz plot in terms of heavy and light invariant masses-squared of the $\pi^\pm \pi^\mp$ systems (denoted m_{max}^2 and m_{min}^2 , respectively), so that each candidate has a uniquely defined position. Moreover, we explicitly enforce the symmetrization of the total amplitude under exchange of identical bosons.

The total signal amplitudes for B^+ and B^- decays are given by

$$A \equiv A(m_{\text{max}}^2, m_{\text{min}}^2) = \sum_j c_j F_j(m_{\text{max}}^2, m_{\text{min}}^2), \quad (1)$$

$$\bar{A} \equiv \bar{A}(m_{\text{max}}^2, m_{\text{min}}^2) = \sum_j \bar{c}_j \bar{F}_j(m_{\text{max}}^2, m_{\text{min}}^2).$$

The complex coefficients c_j and \bar{c}_j for a given decay mode j contain all the weak phase dependence. Since the F_j terms contain only strong dynamics, $F_j \equiv \bar{F}_j$. We use the following parametrization [21] for the amplitude coefficients:

$$c_j = (x_j + \Delta x_j) + i(y_j + \Delta y_j) \quad (2)$$

$$\bar{c}_j = (x_j - \Delta x_j) + i(y_j - \Delta y_j).$$

In this approach, x_j and y_j (Δx_j and Δy_j) are the CP -conserving (-violating) components of the decay amplitude.

The F_j distributions describe the dynamics of the decay amplitudes and are written as the product of an invariant mass term R_j , two Blatt-Weisskopf barrier form factors X_J , and an angular function T_j

$$F_j(m_{\text{max}}^2, m_{\text{min}}^2) \equiv R_j(m) X_J(p^*) X_J(q) T_j(m), \quad (3)$$

where m (J) is the mass (spin) of the resonance, p^* is the momentum the bachelor pion that is not part of the resonance in the B meson rest frame, and q is the momentum

of either daughter in the rest frame of the resonance (we use the $c = 1$ convention for all equations in this paper). The F_j are normalized over the entire Dalitz plot:

$$\iint |F_j(m_{\max}^2, m_{\min}^2)|^2 dm_{\max}^2 dm_{\min}^2 = 1. \quad (4)$$

The Blatt-Weisskopf barrier form factors [33] are given by:

$$\begin{aligned} X_{J=0}(z) &= 1, \\ X_{J=1}(z) &= \sqrt{1/[1 + (z r_{\text{BW}})^2]}, \\ X_{J=2}(z) &= \sqrt{1/[(z r_{\text{BW}})^4 + 3(z r_{\text{BW}})^2 + 9]}, \end{aligned} \quad (5)$$

where the meson radius parameter r_{BW} is taken to be 4.0 ± 1.0 (GeV/c) $^{-1}$ [34].

For most resonances in this analysis the R_j are taken to be relativistic Breit–Wigner lineshapes

$$R_j(m) = \frac{1}{(m_0^2 - m^2) - im_0\Gamma(m)}, \quad (6)$$

where m_0 is the nominal mass of the resonance and $\Gamma(m)$ is the mass-dependent width. In the general case of a spin- J resonance, the latter can be expressed as

$$\Gamma(m) = \Gamma_0 \left(\frac{q}{q_0}\right)^{2J+1} \frac{m_0}{m} \frac{X_J^2(q)}{X_J^2(q_0)}. \quad (7)$$

The symbol Γ_0 denotes the nominal width of the resonance. The values of m_0 and Γ_0 are obtained from standard tables [34] when they are well known. The symbol q_0 denotes the value of q when $m = m_0$.

The angular distribution terms T_j in Eq. (3) follow the Zemach tensor formalism [35, 36]. For the decay of a spin zero B -meson into a spin J resonance and a spin zero bachelor particle this gives [37]

$$\begin{aligned} T_j^{J=0} &= 1, \\ T_j^{J=1} &= -2\vec{p} \cdot \vec{q}, \\ T_j^{J=2} &= \frac{4}{3} [3(\vec{p} \cdot \vec{q})^2 - (|\vec{p}||\vec{q}|)^2], \end{aligned} \quad (8)$$

where \vec{p} is the momentum of the bachelor particle and \vec{q} is the momentum of the resonance daughter with charge opposite from that of the bachelor particle, both measured in the rest frame of the resonance.

The Gounaris–Sakurai parametrization [38] of the P -wave scattering amplitude for a broad resonance decaying to two pions is used for the $\rho^0(770)$ and $\rho^0(1450)$ lineshapes

$$R_j(m) = \frac{1 + \Gamma_0 d/m_0}{(m_0^2 - m^2) + f(m) - im_0\Gamma(m)} \quad (9)$$

where

$$\begin{aligned} f(m) &= \Gamma_0 \frac{m_0^2}{q_0^3} \times \\ &\left[q^2 [h(m) - h(m_0)] + (m_0^2 - m^2) q_0^2 \frac{dh}{dm} \Big|_{m_0} \right], \end{aligned} \quad (10)$$

and the function $h(m)$ is defined as

$$h(m) = \frac{2}{\pi} \frac{q}{m} \ln \left(\frac{m + 2q}{2m_\pi} \right), \quad (11)$$

with

$$\frac{dh}{dm} \Big|_{m_0} = h(m_0) [(8q_0^2)^{-1} - (2m_0^2)^{-1}] + (2\pi m_0^2)^{-1}. \quad (12)$$

The normalization condition at $R_j(0)$ fixes the parameter $d = f(0)/(\Gamma_0 m_0)$. It is found to be

$$d = \frac{3}{\pi} \frac{m_\pi^2}{q_0^2} \ln \left(\frac{m_0 + 2q_0}{2m_\pi} \right) + \frac{m_0}{2\pi q_0} - \frac{m_\pi^2 m_0}{\pi q_0^3}. \quad (13)$$

We model the nonresonant component using an empirical function that has been found to accurately describe nonresonant contributions in other charmless three-body B decays [23, 24, 25, 28, 29]:

$$A_{\text{nr}} = c_{\text{nr}} (e^{-\alpha_{\text{nr}} m_{\max}^2} + e^{-\alpha_{\text{nr}} m_{\min}^2}). \quad (14)$$

We include this term in the coherent sum given by Eq. (1) when calculating the total signal amplitude over the Dalitz plot.

To allow comparison among experiments we present results also in terms of fit fractions (FF_j), defined as the integral of a single decay amplitude squared divided by the total matrix element squared for the complete Dalitz plot

$$FF_j = \frac{\iint (|c_j F_j|^2 + |\bar{c}_j \bar{F}_j|^2) dm_{\max}^2 dm_{\min}^2}{\iint (|A|^2 + |\bar{A}|^2) dm_{\max}^2 dm_{\min}^2}. \quad (15)$$

Note that the sum of all the fit fractions is not necessarily unity due to the possible presence of constructive or destructive interference. The CP asymmetry for each contributing resonance is determined from the fitted parameters

$$\begin{aligned} \mathcal{A}_{CP,j} &= \frac{|\bar{c}_j|^2 - |c_j|^2}{|\bar{c}_j|^2 + |c_j|^2} \\ &= \frac{-2(x_j \Delta x_j + y_j \Delta y_j)}{(x_j)^2 + (\Delta x_j)^2 + (y_j)^2 + (\Delta y_j)^2}. \end{aligned} \quad (16)$$

The signal Dalitz plot probability density function (PDF) is formed from the total amplitude as follows:

$$\begin{aligned} \mathcal{P}_{\text{sig}}(m_{\max}^2, m_{\min}^2, q_B) &= \\ &\frac{\frac{1+q_B}{2} |A|^2 \varepsilon + \frac{1-q_B}{2} |\bar{A}|^2 \bar{\varepsilon}}{\iint (|A|^2 \varepsilon + |\bar{A}|^2 \bar{\varepsilon}) dm_{\max}^2 dm_{\min}^2}, \end{aligned} \quad (17)$$

where q_B is the charge of the B -meson candidate, and $\varepsilon \equiv \varepsilon(m_{\max}^2, m_{\min}^2)$ and $\bar{\varepsilon} \equiv \bar{\varepsilon}(m_{\max}^2, m_{\min}^2)$ are the signal reconstruction efficiencies for B^+ and B^- events, respectively, defined for all points in the Dalitz plot.

CANDIDATE SELECTION

We reconstruct B candidates from events that have four or more charged tracks. Each track is required to be well measured and to originate from the beam spot. They must have a minimum transverse momentum of 50 MeV/ c , and a distance of closest approach to the beam spot of less than 1.5 cm in the transverse plane and less than 2.5 cm along the detector axis. B candidates are formed from combinations of three charged tracks, and particle identification (PID) criteria are applied to reject electrons and to separate pions from kaons. In our final state, the average selection efficiency for pions that have passed the tracking and PID requirements is about 93% including geometrical acceptance, while the average misidentification probability of kaons as pions is close to 8%.

Two kinematic variables are used to identify signal B decays. The first variable is

$$\Delta E = E_B^* - \sqrt{s}/2, \quad (18)$$

the difference between the reconstructed CM energy of the B -meson candidate (E_B^*) and $\sqrt{s}/2$, where \sqrt{s} is the total CM energy. The second is the beam-energy-substituted mass

$$m_{\text{ES}} = \sqrt{s/4 - |\vec{p}_B^*|^2}, \quad (19)$$

where \vec{p}_B^* is the B momentum measured in the CM frame. The m_{ES} distribution for signal events peaks near the B mass with a resolution of around 2.5 MeV/ c^2 , while the ΔE distribution peaks at zero with a resolution of approximately 20 MeV. We initially require events to lie in the region formed by the following selection criteria: $5.200 < m_{\text{ES}} < 5.286$ GeV/ c^2 and $-0.075 < \Delta E < 0.300$ GeV. The region of ΔE below -0.075 GeV is heavily contaminated by four-body B decay backgrounds and is not useful for studying the continuum background. The selected region is then subdivided into three areas: the “left sideband” ($5.20 < m_{\text{ES}} < 5.26$ GeV/ c^2 and $|\Delta E| < 0.075$ GeV) used to study the background ΔE and Dalitz plot distributions; the “upper sideband” ($5.230 < m_{\text{ES}} < 5.286$ GeV/ c^2 and $0.1 < \Delta E < 0.3$ GeV) used to study the background m_{ES} distributions; and the “signal region” ($5.272 < m_{\text{ES}} < 5.286$ GeV/ c^2 and $|\Delta E| < 0.075$ GeV) with which the final fit to data is performed. Following the calculation of these kinematic variables, each of the B candidates is refitted with its mass constrained to the world-average value of the B meson mass [34] in order to improve the Dalitz plot position resolution and to make sure all events lie within the kinematic boundary of the Dalitz plot.

The dominant source of background comes from light-quark and charm continuum production ($e^+e^- \rightarrow q\bar{q}$, where $q = u, d, s, c$). This background is suppressed by requirements on event-shape variables calculated in

the CM frame. We compute a neural network (NN) from the following five variables: the ratio of the second- and zeroth-order angular moments (L_2/L_0), with $L_j = \sum_i p_i |\cos \theta_i|^j$, where θ_i is the angle of the track or neutral cluster i with respect to the signal B thrust axis, p_i is its momentum, and the sum excludes the daughters of the B candidate; the absolute value of the cosine of the angle between the direction of the B and the detector axis; the magnitude of the cosine of the angle between the signal B thrust axis and the detector axis; the output of a multivariate B -flavor tagging algorithm [39] multiplied by the charge of the B candidate; and the ratio of the measured proper time difference of the two B decay vertices and its statistical uncertainty. We train the NN using samples of off-peak data and signal Monte Carlo (MC) events generated with the phase-space distribution. A selection requirement is imposed on the NN output that accepts about 48% of signal events while rejecting 97% of continuum background events.

Dalitz plot distributions of the reconstruction efficiency for B^+ and B^- events are modeled with two-dimensional histograms formed from a sample of around 7×10^6 $B^\pm \rightarrow \pi^\pm \pi^\pm \pi^\mp$ phase-space MC events. All selection criteria are applied except for the exclusion of certain invariant-mass regions described below. We take the ratio of two histograms, the denominator containing the true Dalitz plot distribution of all generated MC events and the numerator containing the reconstructed MC events. The reconstructed events are weighted in order to correct for differences between data and MC simulations in the tracking and PID efficiencies. In order to give better resolution near the edges of the Dalitz plot, where most reconstructed events lie, the histograms are formed in the “square Dalitz plot” [10, 32] coordinates. We use 50×50 bins and smooth these histograms by applying linear interpolation between neighboring bins. The efficiency shows very little variation across most of the Dalitz plot but decreases towards the corners where one of the particles has low momentum. The effect of experimental resolution on the signal model is neglected since the resonances under consideration are sufficiently broad. The average reconstruction efficiency for events in the signal region for the phase-space MC sample is about 15%. The fraction of misreconstructed signal events is only 5%, and MC studies indicate that there is no need for any explicit treatment of these events.

BACKGROUNDS

In addition to the continuum ($q\bar{q}$) background we also have backgrounds from $B\bar{B}$ events. There are four main sources: (i) combinatorial background from three unrelated tracks; (ii) three- and four-body B decays involving an intermediate D meson; (iii) charmless two- and four-body decays with an extra or missing parti-

cle; and (iv) three-body decays with one or more particles misidentified. We reject background from two-body decays of D mesons and charmonium states by excluding invariant masses (in units of GeV/c^2) in the ranges: $1.660 < m_{\pi^+\pi^-} < 1.920$, $3.051 < m_{\pi^+\pi^-} < 3.222$, and $3.660 < m_{\pi^+\pi^-} < 3.820$. These ranges reject decays from $\bar{D}^0 \rightarrow K^+\pi^-$ (or $\pi^+\pi^-$), $J/\psi \rightarrow \ell^+\ell^-$, and $\psi(2S) \rightarrow \ell^+\ell^-$ respectively, where ℓ is a lepton that has been misidentified as a pion. We also employ a special requirement to reject the decay process $B^\pm \rightarrow K_s^0\pi^\pm$; $K_s^0 \rightarrow \pi^+\pi^-$, by excluding candidates where the vertexed mass of two oppositely charged pions lies in the range of $[478, 516] \text{ MeV}/c^2$.

We use a large sample of MC-simulated $B\bar{B}$ decays, equivalent to approximately 3 times the integrated luminosity of the data sample, to identify the important B backgrounds that survive the invariant-mass exclusion requirements described above. In total, 53 B -meson decay modes are identified for which larger samples of exclusive MC events are used for further study. We combine modes that have similar behavior in the discriminating variables m_{ES} and ΔE into a B -background category. There are four such categories: the first contains the two-body decays $B^0 \rightarrow \pi^+\pi^-$ and $B^0 \rightarrow K^-\pi^+$, the second is dominated by $B^\pm \rightarrow K^\pm\pi^\pm\pi^\mp$ and contains other decays with similar topologies, the third contains only $B^0 \rightarrow \pi^+\pi^-\pi^0$, and the fourth contains the remaining backgrounds from B decays that are combinatorial in nature. For each B -background category the combined m_{ES} , ΔE , and Dalitz plot distributions are created where the relative contributions of various decay modes in a specific category are calculated from the reconstruction efficiencies from MC simulations and the branching fractions listed by the Particle Data Group [34] and the Heavy Flavor Averaging Group [40]. These distributions are used in the likelihood fit described below.

Background Dalitz plot distributions are included in the likelihood fit through the use of two-dimensional histograms. For backgrounds from B decays these histograms are formed from the various MC samples. For the continuum background the left sideband data sample is used. Since this data sideband also contains events from B decays, MC samples are used to subtract these events. To these B -subtracted sideband events, we add off-peak data events from across the whole range of m_{ES} and ΔE in order to enhance statistics. We have verified that the shapes of various discriminating variables are compatible between the sideband and off-peak events. As for the reconstruction efficiency histograms, the background Dalitz plot distributions are formed in the square Dalitz plot coordinates and are smoothed by linear interpolation applied between neighboring bins. Separate histograms are constructed for B^+ and B^- events. The $q\bar{q}$ - and B -background PDFs are identical in their con-

struction, and the $q\bar{q}$ PDF is shown here as an example:

$$\mathcal{P}_{q\bar{q}}(m_{\text{max}}^2, m_{\text{min}}^2, q_B) = \frac{1}{2}(1 - q_B \mathcal{A}_{q\bar{q}}) \times \quad (20)$$

$$\left(\frac{\frac{1+q_B}{2} Q(m_{\text{max}}^2, m_{\text{min}}^2)}{\iint Q(m_{\text{max}}^2, m_{\text{min}}^2) dm_{\text{max}}^2 dm_{\text{min}}^2} + \frac{\frac{1-q_B}{2} \bar{Q}(m_{\text{max}}^2, m_{\text{min}}^2)}{\iint \bar{Q}(m_{\text{max}}^2, m_{\text{min}}^2) dm_{\text{max}}^2 dm_{\text{min}}^2} \right),$$

where $\mathcal{A}_{q\bar{q}}$ is the charge asymmetry in the background, and $Q(m_{\text{max}}^2, m_{\text{min}}^2)$ and $\bar{Q}(m_{\text{max}}^2, m_{\text{min}}^2)$ are the Dalitz plot distributions of $q\bar{q}$ events in selected B^+ and B^- samples, respectively.

MAXIMUM LIKELIHOOD FIT

To provide further discrimination between the signal and background hypotheses in the likelihood fit, we include PDFs for the kinematic variables m_{ES} and ΔE , which multiply that of the Dalitz plot. The signal m_{ES} shape is modeled with the sum of a Gaussian function and a Crystal-Ball lineshape [41], and the ΔE shape is modeled with a double Gaussian function. The parameters of these functions are obtained from a sample of $B^\pm \rightarrow \pi^\pm\pi^\pm\pi^\mp$ MC events, modeled according to the Dalitz plot distribution from Ref. [32], and are appropriately adjusted to account for possible differences between data and MC simulations determined with a control sample of $B^+ \rightarrow \bar{D}^0\pi^+$; $\bar{D}^0 \rightarrow K^+\pi^-$ decays. These parameters are fixed in the fit to data.

The $q\bar{q}$ m_{ES} distribution is modeled with the experimentally motivated ARGUS function [42]. The end point for the ARGUS function is fixed to $5.289 \text{ GeV}/c^2$, and the parameter describing the shape is fixed to the value determined from the combined sample of upper sideband and off-peak data. We model the continuum ΔE shape using a linear function, the slope of which is fixed to the value determined from the left sideband and off-peak data. The $B\bar{B}$ background distributions are modeled with histograms obtained from the mixture of $B\bar{B}$ MC samples. The yields of signal and $q\bar{q}$ events are allowed to vary in the final fit to the data while the yields of $B\bar{B}$ backgrounds are fixed to 11 (two-body decays), 195 ($B^\pm \rightarrow K^\pm\pi^\pm\pi^\mp$ type), 117 ($B^0 \rightarrow \pi^+\pi^-\pi^0$), and 495 (combinatorial) events.

The complete likelihood function is given by:

$$\mathcal{L} = e^{-N} \times \quad (21)$$

$$\prod_j^{N_e} \left[\sum_k N_k \mathcal{P}_k^j(m_{\text{max}}^2, m_{\text{min}}^2, m_{\text{ES}}, \Delta E, q_B) \right],$$

where N is equal to $\sum_k N_k$, N_k is the yield for the event category k , N_e is the total number of events in the data sample, and \mathcal{P}_k^j is the PDF for the category k for event j , which consists of a product of the Dalitz plot, m_{ES} , and ΔE PDFs. The function $-2 \ln \mathcal{L}$ is minimized in an unbinned fit to the data.

Our nominal signal Dalitz plot model comprises a momentum-dependent nonresonant component and four intermediate resonance states: $\rho^0(770)\pi^\pm$, $\rho^0(1450)\pi^\pm$, $f_2(1270)\pi^\pm$, and $f_0(1370)\pi^\pm$. The parameters used to describe these states are summarized in Table I. We fit 4335 B candidates in the signal region selected from the data to obtain the central values of the x_j , Δx_j , y_j , and Δy_j parameters for each component, and use Eqs. (15) and (16) to calculate the fit fractions and CP asymmetries. We use $\rho^0(770)\pi^\pm$ as the reference amplitude, fixing its x , y , and Δy parameters to unity, zero, and zero, respectively. The signal yield, $q\bar{q}$ background yield and asymmetry are also free parameters of the fit, giving a total of 20 free parameters.

The Dalitz plot model was determined using the results of our previous analysis [32] and the changes in the fit likelihood and χ^2 values when omitting or adding resonances. The latter is calculated from the projection of the fit results onto the Dalitz plot using the formula

$$\chi^2 = \sum_{i=1}^{n_b} \frac{[y_i - f(x_i)]^2}{f(x_i)}, \quad (22)$$

where y_i is the number of data events in bin i and $f(x_i)$ is the number of events in that bin as predicted by the fit result. The number of degrees of freedom is calculated as $n_b - h - 1$, where n_b is the total number of bins used and h is the number of free parameters in the fit. A minimum of 20 entries in each bin is required; if this requirement is not met then the neighboring bins are combined. Typically, n_b takes values around 100.

In our previous study we found significant contributions from $\rho^0(770)\pi^\pm$ and $f_2(1270)\pi^\pm$; with $f_0(980)\pi^\pm$, $\rho^0(1450)\pi^\pm$, and a uniform nonresonant term also included in the model. Because of the larger data sample and many improvements to the analysis, we find it necessary to include an additional contribution from $f_0(1370)\pi^\pm$, and to use a momentum-dependent nonresonant amplitude [see Eq. (14)] in order to achieve a reasonable agreement of the fit with the data. We do not find any significant signal from $f_0(980)\pi^\pm$, so we exclude this channel from our nominal model and calculate an upper limit for its fit fraction. The statistical significance of the presence of a component is estimated by evaluating the difference $\Delta \ln \mathcal{L}$ between the negative log-likelihood of the nominal fit and that of a fit where all of the x , y , Δx , and Δy parameters for the given component are fixed to zero. This is then used to evaluate a p value

$$p = \int_{2\Delta \ln \mathcal{L}}^{\infty} f(z; n_d) dz, \quad (23)$$

where $f(z; n_d)$ is the PDF of the χ^2 distribution and n_d is the number of degrees of freedom, four in this case. We then determine the equivalent one-dimensional significance from this p value. We find that the $f_2(1270)$ contribution has a statistical significance of 6.1σ , the $\rho^0(1450)$ 4.6σ and the $f_0(1370)$ 3.9σ .

Since the mass and width of the $f_0(1370)$ state are not well known [34], we determine the preferred values from data by scanning the likelihood values obtained with different parameters. The mass and width are determined to be $m_{f_0(1370)} = 1400 \pm 40 \text{ MeV}/c^2$ and $\Gamma_{f_0(1370)} = 300 \pm 80 \text{ MeV}$, with a correlation of $(-39 \pm 4)\%$, where the errors are statistical only, and are obtained from a fit to the two-dimensional likelihood profile. Similarly, we determine the parameter of the nonresonant lineshape to be $\alpha_{nr} = 0.28 \pm 0.06 \text{ GeV}^{-2}c^4$ (statistical uncertainties only).

Possible contributions from $\chi_{c0}\pi^\pm$ and $\chi_{c2}\pi^\pm$ are not significant so we set upper limits on their branching fractions. Furthermore, we do not find any evidence for a very broad enhancement at low $\pi^+\pi^-$ invariant mass such as could be caused by the decay $B^\pm \rightarrow \sigma\pi^\pm$.

TABLE I: Parameters used to describe intermediate states in our nominal model. GS and RBW refer to the Gounaris-Sakurai and relativistic Breit-Wigner lineshapes, respectively.

Resonance	Lineshape	Mass (MeV/ c^2)	Width (MeV)	Ref.
$\rho^0(770)$	GS	775.49 ± 0.34	149.4 ± 1.0	[34]
$\rho^0(1450)$	GS	1465 ± 25	400 ± 60	[34]
$f_2(1270)$	RBW	1275.1 ± 1.2	$185.0^{+2.9}_{-2.4}$	[34]
$f_0(1370)$	RBW	1400 ± 40	300 ± 80	See text

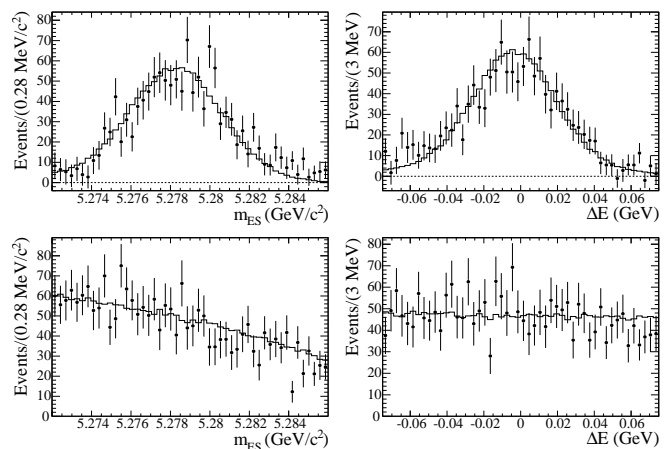


FIG. 1: (Top) signal and (bottom) $q\bar{q}$ distributions of (left) m_{ES} and (right) ΔE obtained from the fit to data using event-by-event signal and $q\bar{q}$ background probabilities [43]. The solid lines show the PDF shapes used in the fit.

Figure 1 shows the m_{ES} and ΔE distributions of signal and $q\bar{q}$ background determined from the fit with event-by-event signal and $q\bar{q}$ background probabilities for each

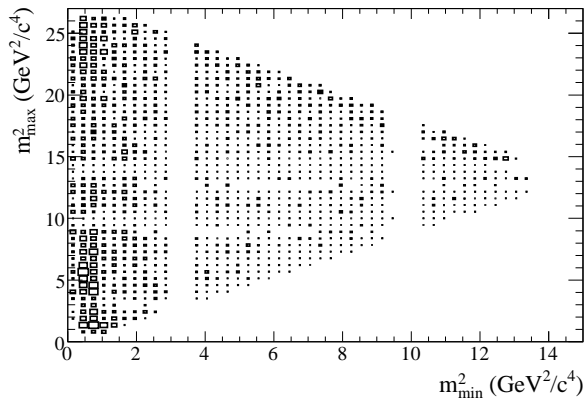


FIG. 2: Background-subtracted Dalitz plot of the combined $B^\pm \rightarrow \pi^\pm \pi^\pm \pi^\mp$ data sample in the signal region. The plot shows bins with greater than zero entries. The area of the boxes is proportional to the number of entries. The depleted bands are the charm and charmonia exclusion regions.

candidate event [43]. The background-subtracted Dalitz plot of the data in the signal region can be seen in Fig. 2. The χ^2 per number of degrees of freedom of the projection of the fit result onto the Dalitz plot is 82/84. Using the fitted signal distribution we calculate the average reconstruction efficiency for our signal sample to be 18%.

We generate a large number of MC experiments with the fitted parameters, and from the spread of results of fits to those experiments we determine the statistical uncertainties on the parameters, FF_j , and $\mathcal{A}_{CP,j}$. This procedure takes into account correlations between the x_j , Δx_j , y_j , and Δy_j parameters. The linear correlation coefficients between the FF_j and $\mathcal{A}_{CP,j}$ parameters are also obtained and are presented in Appendix . In order to calculate the branching fraction for an intermediate mode, we multiply the fit fraction of the latter by the total inclusive $B^\pm \rightarrow \pi^\pm \pi^\pm \pi^\mp$ branching fraction. They are needed for comparison with previous measurements and theoretical predictions. The $\pi^\pm \pi^\pm \pi^\mp$ signal yield is found to be $1219 \pm 50 \pm 75^{+29}_{-24}$ events and the inclusive CP asymmetry to be $(+3.2 \pm 4.4 \pm 3.1^{+2.5}_{-2.0})\%$, where the uncertainties are statistical, systematic, and model-dependent, respectively. Additionally, the total yield and CP asymmetry of the continuum background are found to be 2337 ± 62 events and $(+0.2 \pm 2.7)\%$, respectively, where the uncertainties are statistical only. Further results are shown in Tables II and III.

Projections of the data, with the fit result overlaid, as $\pi^\pm \pi^\mp$ invariant-mass distributions can be seen in Fig. 3. A detailed examination of possible direct CP violation effects in the low $\pi^\pm \pi^\mp$ invariant-mass region is shown in Fig. 4, where we have subdivided the data into positive and negative values of $\cos \theta_H = \vec{p} \cdot \vec{q} / (|\vec{p}| |\vec{q}|)$, where θ_H is the helicity angle, \vec{p} is the momentum of the bachelor par-

ticle and \vec{q} is the momentum of the resonance daughter with charge opposite from that of the bachelor particle, both measured in the rest frame of the resonance. The agreement between the fit result and the data is generally good; the χ^2 per number of non-zero bins for these plots varies between 35/46 and 34/24.

We calculate 90% confidence-level (CL) upper limits for components not included in the nominal Dalitz plot model. These are obtained by generating many MC experiments from the results of fits to the data where the extra component is added to the nominal Dalitz plot model, with all major systematic sources varied within their 1σ uncertainties. We fit these MC samples and plot the fit fraction distributions. The 90% CL upper limit for each fit fraction is the value which includes 90% of the MC experiments. The branching fraction upper limit is then the product of the fit fraction upper limit and the total branching fraction for $B^\pm \rightarrow \pi^\pm \pi^\pm \pi^\mp$.

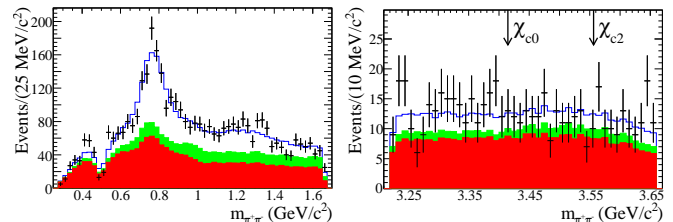


FIG. 3: (color online) Dipion invariant mass projections: (left) in the $\rho^0(770)$ region; and (right) in the regions of χ_{c0} and χ_{c2} . The data are the points with statistical error bars, the dark-shaded (red) histogram is the $q\bar{q}$ component, the light-shaded (green) histogram is the $B\bar{B}$ background contribution, while the upper (blue) histogram shows the total fit result. The dip near $0.5 \text{ GeV}/c^2$ in the left plot is due to the rejection of events containing K_S^0 candidates.

We have searched for the presence of multiple solutions in the fit to data with the nominal model. We find a second solution with a value of $-2 \ln \mathcal{L}$ about ten units higher than our nominal fit, and with a χ^2 of the Dalitz plot projection increased by four units. A comparison of the results between the two solutions is given in Appendix . The most significant difference is seen in the $f_0(1370)$ fit fraction, which is much smaller in the second solution. In Dalitz plot analyses of $K\pi\pi$ and KKK final states [20, 21, 22, 23, 24, 25, 28, 29], similar phenomena relating to multiple solutions have been observed, and interpreted as being due to differences in the possible interference pattern – constructive or destructive interference – between nonresonant and broad amplitudes. Interference between the nonresonant and $f_0(1370)$ amplitudes appears to be a plausible explanation for the effect in this analysis. As can be seen in Fig. 4, the data exhibit a non-trivial interference pattern, and the difficulty in modeling this effect leads to model uncertainties in our results.

TABLE II: Results of fits to data, with statistical, systematic and model-dependent uncertainties.

Resonance	x	y	Δx	Δy
$\rho^0(770)\pi^\pm$	1.0 (fixed)	0.0 (fixed)	$-0.092 \pm 0.036 \pm 0.027$ $^{+0.071}_{-0.012}$	0.0 (fixed)
$\rho^0(1450)\pi^\pm$	$-0.292 \pm 0.071 \pm 0.065$ $^{+0.182}_{-0.054}$	$0.175 \pm 0.078 \pm 0.048$ $^{+0.133}_{-0.042}$	$0.109 \pm 0.080 \pm 0.059$ $^{+0.038}_{-0.116}$	$0.211 \pm 0.073 \pm 0.038$ $^{+0.032}_{-0.146}$
$f_2(1270)\pi^\pm$	$0.136 \pm 0.064 \pm 0.040$ $^{+0.178}_{-0.029}$	$0.149 \pm 0.052 \pm 0.030$ $^{+0.022}_{-0.077}$	$0.101 \pm 0.063 \pm 0.016$ $^{+0.031}_{-0.183}$	$-0.248 \pm 0.052 \pm 0.024$ $^{+0.024}_{-0.026}$
$f_0(1370)\pi^\pm$	$0.397 \pm 0.067 \pm 0.058$ $^{+0.047}_{-0.050}$	$-0.151 \pm 0.081 \pm 0.052$ $^{+0.057}_{-0.187}$	$-0.387 \pm 0.064 \pm 0.029$ $^{+0.072}_{-0.082}$	$-0.168 \pm 0.086 \pm 0.055$ $^{+0.160}_{-0.046}$
Nonresonant	$-0.200 \pm 0.091 \pm 0.029$ $^{+0.239}_{-0.045}$	$-0.682 \pm 0.070 \pm 0.038$ $^{+0.032}_{-0.082}$	$-0.392 \pm 0.089 \pm 0.055$ $^{+0.037}_{-0.128}$	$0.046 \pm 0.069 \pm 0.055$ $^{+0.101}_{-0.124}$

TABLE III: Summary of measurements of branching fractions (averaged over charge conjugate states) and CP asymmetries. The first error is statistical, the second is systematic and the third represents the model dependence. Also included are 90% CL upper limits of the branching fractions of the components that do not have statistically significant fit fractions.

Mode	Fit Fraction (%)	$\mathcal{B}(B^\pm \rightarrow \text{Mode})(10^{-6})$	\mathcal{A}_{CP} (%)
$\pi^\pm \pi^\pm \pi^\mp$ Total	-	$15.2 \pm 0.6 \pm 1.2$ $^{+0.4}_{-0.3}$	$+3.2 \pm 4.4 \pm 3.1$ $^{+2.5}_{-2.0}$
$\rho^0(770)\pi^\pm; \rho^0(770) \rightarrow \pi^+\pi^-$	$53.2 \pm 3.7 \pm 2.5$ $^{+1.5}_{-7.4}$	$8.1 \pm 0.7 \pm 1.2$ $^{+0.4}_{-1.1}$	$+18 \pm 7 \pm 5$ $^{+2}_{-14}$
$\rho^0(1450)\pi^\pm; \rho^0(1450) \rightarrow \pi^+\pi^-$	$9.1 \pm 2.3 \pm 2.4$ $^{+1.9}_{-4.5}$	$1.4 \pm 0.4 \pm 0.4$ $^{+0.3}_{-0.7}$	$-6 \pm 28 \pm 20$ $^{+12}_{-35}$
$f_2(1270)\pi^\pm; f_2(1270) \rightarrow \pi^+\pi^-$	$5.9 \pm 1.6 \pm 0.4$ $^{+2.0}_{-0.7}$	$0.9 \pm 0.2 \pm 0.1$ $^{+0.3}_{-0.1}$	$+41 \pm 25 \pm 13$ $^{+12}_{-8}$
$f_0(1370)\pi^\pm; f_0(1370) \rightarrow \pi^+\pi^-$	$18.9 \pm 3.3 \pm 2.6$ $^{+4.3}_{-3.5}$	$2.9 \pm 0.5 \pm 0.5$ $^{+0.7}_{-0.5}$ (< 4.0)	$+72 \pm 15 \pm 14$ $^{+7}_{-8}$
$\pi^\pm \pi^\pm \pi^\mp$ nonresonant	$34.9 \pm 4.2 \pm 2.9$ $^{+7.5}_{-3.4}$	$5.3 \pm 0.7 \pm 0.6$ $^{+1.1}_{-0.5}$	$-14 \pm 14 \pm 7$ $^{+17}_{-3}$
$f_0(980)\pi^\pm; f_0(980) \rightarrow \pi^+\pi^-$	-	< 1.5	-
$\chi_{c0}\pi^\pm; \chi_{c0} \rightarrow \pi^+\pi^-$	-	< 0.1	-
$\chi_{c2}\pi^\pm; \chi_{c2} \rightarrow \pi^+\pi^-$	-	< 0.1	-

SYSTEMATIC UNCERTAINTIES

Systematic uncertainties that affect the measurement of fit fractions, phases, event yields, and CP asymmetries are summarized in Table IV. The fixed $B\bar{B}$ -background yields and asymmetries are allowed to vary and the variations of the other fitted parameters are taken as the uncertainties. The effect of limited statistics of the data sideband and MC samples used to obtain the fixed shapes of all the histogram PDFs is accounted for by fluctuating independently the histogram bin contents in accordance with their errors and repeating the nominal fit. The uncertainties on how well the samples model these distributions are also taken into account through various cross-checks, including variation of the mass rejection ranges and comparison of continuum shapes between sideband and signal region in MC samples.

The fixed parameters of the signal m_{ES} and ΔE PDFs are studied in the control sample $B^+ \rightarrow \bar{D}^0 \pi^+$; $\bar{D}^0 \rightarrow K^+ \pi^-$. The parameters are determined from data and MC samples, from which shift and scale factors are calculated and used to adjust the parameters for the nominal fit. The parameters are then varied in accordance with the errors on these shift and scale factors and the

fits are repeated. Uncertainties due to the m_{ES} distribution for the $q\bar{q}$ background, which is fixed in the fit, are assessed to be negligible. The fit confirms the value of the single parameter of the ARGUS function that is taken as input.

To confirm the fitting procedure, we perform 500 MC experiments in which the events are generated from the PDFs used in the fit to data. We repeat the exercise with $q\bar{q}$ events alone drawn from the PDF into which we embed signal and $B\bar{B}$ background events randomly extracted from the MC samples. Small fit biases are observed for some of the fit parameters and are included in the systematic uncertainties.

Relative uncertainties in the efficiency, due to PID and tracking efficiency corrections are 4.2% and 2.4% respectively; while $N_{B\bar{B}}$ has an associated error of 1.1%. The efficiency correction due to the selection requirement on the NN output has also been calculated from $B^+ \rightarrow \bar{D}^0 \pi^+$; $\bar{D}^0 \rightarrow K^+ \pi^-$ data and MC samples, and is found to be $(96.2 \pm 1.2)\%$. The error on this correction is incorporated into the branching fraction systematic uncertainties.

Measured CP asymmetries could be affected by detector charge bias. We include a systematic uncertainty of 0.005 to account for this effect [21]. Furthermore, some

TABLE IV: Absolute maximum values of the systematic uncertainties for the amplitude coefficients, fit fractions, signal yield, and CP asymmetries from various sources described in the text.

Source	x	y	Δx	Δy	Fit fraction	\mathcal{A}_{CP}	Signal yield	Signal asymmetry
$B\bar{B}$ yields	0.02	0.04	0.02	...	0.02	0.08	1.4	0.01
$B\bar{B}$ PDF	0.01	3.3	...
Signal PDF	0.02	0.02	0.01	0.02	0.01	0.08	48.3	0.01
$q\bar{q}$ Dalitz plot	0.06	0.03	0.05	0.05	0.03	0.14	47.7	...
$B\bar{B}$ Dalitz plot	0.03	0.03	0.02	0.02	0.02	0.10	31.6	0.02
Efficiency Dalitz plot	...	0.01	0.03	0.6	...
Fit bias	0.01	0.02	0.02	0.01	...	0.05	2.8	...

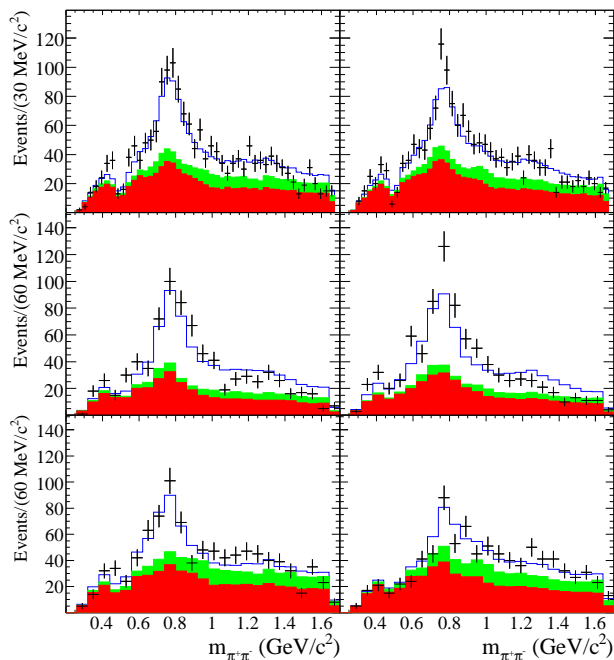


FIG. 4: (color online) Dipion invariant mass projection in the $\rho^0(770)$ region for (left) B^- and (right) B^+ candidates. The top row shows all candidates, the middle row shows those with $\cos\theta_H > 0$ and the bottom row shows those with $\cos\theta_H < 0$. The colors and shadings follow the same convention as Fig. 3.

of our selection requirements, for example that on the NN output, may induce an asymmetry. We estimate the possible size of such an effect as 0.020 based on the study of our control sample.

In addition to the above systematic uncertainties we also estimate uncertainties from two sources related to the signal Dalitz plot model. The first of these elements consists of the parameters of the various components of the signal model: the masses and widths of all intermediate resonances, the value of the parameter that characterizes the nonresonant shape, and the value of the

Blatt–Weisskopf barrier radius. The associated uncertainties are evaluated by adjusting the parameters within their experimental errors and refitting. The second element is the uncertainty due to the composition of the signal model. It reflects observed changes in the parameters of the components when the data are fitted with the less significant $f_0(1370)$ component removed from the model and with one of the states $\omega(782)$, $f_0(980)$, χ_{c0} , or χ_{c2} added to the model. The uncertainties from each of these elements are added in quadrature to obtain the final model-dependence.

DISCUSSION AND SUMMARY

Our results are shown in Tables II and III. The Dalitz plot is dominated by the $\rho^0(770)$ resonance and a non-resonant contribution which, as seen in other charmless three-body hadronic B decays, is well modeled with an exponential form-factor. The measured branching fraction for the decay $B^\pm \rightarrow \rho^0(770)\pi^\pm$ agrees with the world-average value [34] and is consistent with theoretical predictions based on QCD factorization models [44] and SU(3) flavor symmetry [45]. The measured branching fraction of the nonresonant lineshape is consistent with some theoretical predictions [14, 16, 17]. We find the parameter of the nonresonant lineshape to be $\alpha_{nr} = 0.28 \pm 0.06 \text{ GeV}^{-2}c^4$ (statistical uncertainties only), which is comparable with values found in analyses of other charmless decay modes such as $B \rightarrow K\pi\pi$ [23, 24, 25] and $B \rightarrow KKK$ [23, 28].

Contributions from $\rho^0(1450)$ and $f_0(1370)$ are also included in the Dalitz plot model, where the mass and width of the $f_0(1370)$ are determined to be $m_{f_0(1370)} = 1400 \pm 40 \text{ MeV}/c^2$ and $\Gamma_{f_0(1370)} = 300 \pm 80 \text{ MeV}$ (statistical uncertainties only). We have made the first observation of the decay $B^\pm \rightarrow f_2(1270)\pi^\pm$ with a statistical significance of 6.1σ . After correcting for the $f_2(1270) \rightarrow \pi^+\pi^-$

branching fraction of $(84.8_{-1.2}^{+2.4}) \times 10^{-2} \times \frac{2}{3}$ [34], we obtain

$$\mathcal{B}(B^\pm \rightarrow f_2(1270)\pi^\pm) = (1.57 \pm 0.42 \pm 0.16_{-0.19}^{+0.53}) \times 10^{-6} \quad (24)$$

where the uncertainties are statistical, systematic, and model-dependent, respectively. The latter includes the uncertainty of the $f_2(1270) \rightarrow \pi^+\pi^-$ branching fraction. The above measurements of the branching fractions are generally improved from previous results [32], although some of the uncertainties are not reduced, largely due to a more realistic assignment of model-dependent uncertainties in this analysis.

The 90% confidence-level upper limits for the branching fractions of $B^\pm \rightarrow \chi_{c0}\pi^\pm$ and $B^\pm \rightarrow \chi_{c2}\pi^\pm$ are found to be

$$\mathcal{B}(B^\pm \rightarrow \chi_{c0}\pi^\pm) < 1.5 \times 10^{-5} \quad (25)$$

$$\mathcal{B}(B^\pm \rightarrow \chi_{c2}\pi^\pm) < 2.0 \times 10^{-5} \quad (26)$$

where the $\chi_{c(0,2)} \rightarrow \pi^+\pi^-$ widths are determined from recent measurements by Belle [46]. The absence of these charmonium contributions precludes the extraction of the unitarity triangle angle γ that has been proposed in the literature [3, 4, 5, 6, 7, 8].

We do not find any signal for the decay $B^\pm \rightarrow f_0(980)\pi^\pm$. The branching fraction upper limit we obtain is consistent with the prediction of a recent perturbative QCD calculation if the $f_0(980)$ meson is dominated by an $s\bar{s}$ component [47].

We do not find any statistically significant CP asymmetries for the components in the nominal Dalitz plot model. The CP asymmetry in $B^\pm \rightarrow \rho^0(770)\pi^\pm$ has a dependence on the presence or absence of the $f_0(1370)$ term in the model. The CP asymmetry of the $f_0(1370)$ term itself appears highly sensitive to the Dalitz plot model, varying dramatically between the favored and the second solution. Since the presence of this component is not established, especially given its insignificant contribution in the second solution, we set a 90% CL upper limit on its product branching fraction at 4.0×10^{-6} .

In conclusion, we have performed a Dalitz plot analysis of $B^\pm \rightarrow \pi^\pm\pi^\pm\pi^\mp$ decays based on a 424fb^{-1} data sample containing $(465 \pm 5) \times 10^6$ $B\bar{B}$ pairs collected with the *BABAR* detector. Our model includes a momentum-dependent nonresonant component and four intermediate resonance states: $\rho^0(770)\pi^\pm$, $\rho^0(1450)\pi^\pm$, $f_2(1270)\pi^\pm$, and $f_0(1370)\pi^\pm$. We do not find any significant contributions from $f_0(980)\pi^\pm$, $\chi_{c0}\pi^\pm$, or $\chi_{c2}\pi^\pm$. We find no evidence for direct CP violation. Our results will be useful to reduce model uncertainties in the extraction of the CKM angle α from time-dependent Dalitz plot analysis of $B^0 \rightarrow \pi^+\pi^-\pi^0$. The results presented here supersede those in our previous publication [32].

ACKNOWLEDGMENTS

We are grateful for the extraordinary contributions of our PEP-II colleagues in achieving the excellent luminosity and machine conditions that have made this work possible. The success of this project also relies critically on the expertise and dedication of the computing organizations that support *BABAR*. The collaborating institutions wish to thank SLAC for its support and the kind hospitality extended to them. This work is supported by the US Department of Energy and National Science Foundation, the Natural Sciences and Engineering Research Council (Canada), the Commissariat à l'Énergie Atomique and Institut National de Physique Nucléaire et de Physique des Particules (France), the Bundesministerium für Bildung und Forschung and Deutsche Forschungsgemeinschaft (Germany), the Istituto Nazionale di Fisica Nucleare (Italy), the Foundation for Fundamental Research on Matter (The Netherlands), the Research Council of Norway, the Ministry of Education and Science of the Russian Federation, Ministerio de Educación y Ciencia (Spain), and the Science and Technology Facilities Council (United Kingdom). Individuals have received support from the Marie-Curie IEF program (European Union) and the A. P. Sloan Foundation.

* Deceased

† Now at Temple University, Philadelphia, PA 19122, USA

‡ Now at Tel Aviv University, Tel Aviv, 69978, Israel

§ Also with Università di Perugia, Dipartimento di Fisica, Perugia, Italy

¶ Also with Università di Roma La Sapienza, I-00185 Roma, Italy

** Now at University of South Alabama, Mobile, AL 36688, USA

†† Also with Laboratoire de Physique Nucléaire et de Hautes Energies, IN2P3/CNRS, Université Pierre et Marie Curie-Paris6, Université Denis Diderot-Paris7, F-75252 Paris, France

‡‡ Also with Università di Sassari, Sassari, Italy

[1] N. Cabibbo, Phys. Rev. Lett. **10**, 531 (1963).

[2] M. Kobayashi and T. Maskawa, Prog. Theor. Phys. **49**, 652 (1973).

[3] G. Eilam, M. Gronau, and R. R. Mendel, Phys. Rev. Lett. **74**, 4984 (1995).

[4] N. G. Deshpande, G. Eilam, X. G. He, and J. Trampetic, Phys. Rev. D **52**, 5354 (1995).

[5] I. Bediaga, R. E. Blanco, C. Gobel, and R. Mendez-Galain, Phys. Rev. Lett. **81**, 4067 (1998).

[6] B. Bajc, S. Fajfer, R. J. Oakes, T. N. Pham, and S. Prelovsek, Phys. Lett. B **447**, 313 (1999).

[7] A. Deandrea, R. Gatto, M. Ladisa, G. Nardulli, and P. Santorelli, Phys. Rev. D **62**, 114011 (2000).

[8] R. E. Blanco, C. Gobel, and R. Mendez-Galain, Phys. Rev. Lett. **86**, 2720 (2001).

[9] A. E. Snyder and H. R. Quinn, Phys. Rev. D **48**, 2139 (1993).

- [10] B. Aubert *et al.* (BABAR Collaboration), Phys. Rev. D **76**, 012004 (2007).
- [11] A. Kusaka *et al.* (Belle Collaboration), Phys. Rev. Lett. **98**, 221602 (2007).
- [12] A. Kusaka *et al.* (Belle Collaboration), Phys. Rev. D **77**, 072001 (2008).
- [13] O. M. A. Leitner, X. H. A. Guo, and A. W. Thomas, Eur. Phys. J. C **31**, 215 (2003).
- [14] A. Deandrea and A. D. Polosa, Phys. Rev. Lett. **86**, 216 (2001).
- [15] S. Gardner and U. G. Meissner, Phys. Rev. D **65**, 094004 (2002).
- [16] J. Tandean and S. Gardner, Phys. Rev. D **66**, 034019 (2002).
- [17] H. Y. Cheng and K. C. Yang, Phys. Rev. D **66**, 054015 (2002).
- [18] U. G. Meissner and S. Gardner, Eur. Phys. J. A **18**, 543 (2003).
- [19] H. Y. Cheng, C. K. Chua, and A. Soni, Phys. Rev. D **76**, 094006 (2007).
- [20] B. Aubert *et al.* (BABAR Collaboration), Phys. Rev. D **72**, 072003 (2005) [Erratum-ibid. D **74**, 099903 (2006)].
- [21] B. Aubert *et al.* (BABAR Collaboration), Phys. Rev. D **78**, 012004 (2008).
- [22] B. Aubert *et al.* (BABAR Collaboration), arXiv:0708.2097.
- [23] A. Garmash *et al.* (Belle Collaboration), Phys. Rev. D **71**, 092003 (2005).
- [24] A. Garmash *et al.* (Belle Collaboration), Phys. Rev. Lett. **96**, 251803 (2006).
- [25] A. Garmash *et al.* (Belle Collaboration), Phys. Rev. D **75**, 012006 (2007).
- [26] B. Aubert *et al.* (BABAR Collaboration), Phys. Rev. Lett. **99**, 221801 (2007).
- [27] B. Aubert *et al.* (BABAR Collaboration), Phys. Rev. D **79**, 051101 (2009).
- [28] B. Aubert *et al.* (BABAR Collaboration), Phys. Rev. D **74**, 032003 (2006).
- [29] B. Aubert *et al.* (BABAR Collaboration), Phys. Rev. Lett. **99**, 161802 (2007).
- [30] B. Aubert *et al.* (BABAR Collaboration), Nucl. Instrum. Methods Phys. Res., Sect. A **479**, 1 (2002).
- [31] W. Kozanecki, Nucl. Instrum. Methods Phys. Res., Sect. A **446**, 59 (2000).
- [32] B. Aubert *et al.* (BABAR Collaboration), Phys. Rev. D **72**, 052002 (2005).
- [33] J. Blatt and V. E. Weisskopf, *Theoretical Nuclear Physics* (J. Wiley & Sons, New York, 1952).
- [34] C. Amsler *et al.* (Particle Data Group), Phys. Lett. B **667**, 1 (2008). Online updates at <http://pdglive.lbl.gov/>.
- [35] C. Zemach, Phys. Rev. **133**, B1201 (1964).
- [36] C. Zemach, Phys. Rev. **140**, B97 (1965).
- [37] D. Asner (2003), arXiv: hep-ex/0410014.
- [38] G. J. Gounaris and J. J. Sakurai, Phys. Rev. Lett. **21**, 244 (1968).
- [39] B. Aubert *et al.* (BABAR Collaboration), Phys. Rev. Lett. **94**, 161803 (2005).
- [40] E. Barberio *et al.* (Heavy Flavor Averaging Group), arXiv:0808.1297.
- [41] M. J. Oreglia, Ph.D. Thesis, Stanford University [SLAC Report No. R-236, 1980], Appendix D; J. E. Gaiser, Ph.D. Thesis, Stanford University [SLAC Report No. R-255, 1982], Appendix F; and T. Skwarnicki, Ph.D. Thesis, Institute of Nuclear Physics [DESY Report No. F31-86-02, 1986], Appendix E.
- [42] H. Albrecht *et al.* (ARGUS Collaboration), Phys. Lett. B **241**, 278 (1990).
- [43] M. Pivk and F. R. Le Diberder, Nucl. Instrum. Methods Phys. Res., Sect. A **555**, 356 (2005).
- [44] X. Q. Li and Y. D. Yang, Phys. Rev. D **73**, 114027 (2006).
- [45] C. W. Chiang and Y. F. Zhou (2008), J. High Energy Phys. **03** (2009) 055.
- [46] H. Nakazawa *et al.* (Belle Collaboration), Phys. Lett. B **615**, 39 (2005).
- [47] Z. Q. Zhang and Z. J. Xiao, arXiv:0812.2314.

CORRELATIONS BETWEEN FIT FRACTIONS AND DIRECT CP ASYMMETRIES

In Table V we present the statistical linear correlations between the values of FF_j and $\mathcal{A}_{CP,j}$.

COMPARISON OF RESULTS IN FAVORED AND SECOND SOLUTION

In Table VI we give a comparison of the results for the two solutions. Note that the \mathcal{A}_{CP} value of $f_0(1370)\pi^\pm$ is at the physical boundary in the second solution.

TABLE V: Matrix of statistical correlation coefficients between fit fractions and direct CP asymmetries.

Parameter	$\rho^0(770)$		$\rho^0(1450)$		$f_2(1270)$		$f_0(1370)$		Nonresonant	
	FF	\mathcal{A}_{CP}	FF	\mathcal{A}_{CP}	FF	\mathcal{A}_{CP}	FF	\mathcal{A}_{CP}	FF	\mathcal{A}_{CP}
$\rho^0(770) FF$	1.00									
$\rho^0(770) \mathcal{A}_{CP}$	0.00	1.00								
$\rho^0(1450) FF$	0.10	0.29	1.00							
$\rho^0(1450) \mathcal{A}_{CP}$	0.35	0.14	0.31	1.00						
$f_2(1270) FF$	-0.14	-0.02	-0.15	-0.05	1.00					
$f_2(1270) \mathcal{A}_{CP}$	-0.12	0.06	-0.01	-0.02	-0.08	1.00				
$f_0(1370) FF$	-0.28	-0.16	-0.45	-0.31	-0.09	0.02	1.00			
$f_0(1370) \mathcal{A}_{CP}$	-0.14	0.00	-0.09	-0.13	0.01	-0.10	-0.14	1.00		
Nonresonant FF	-0.50	0.06	-0.15	0.06	-0.17	0.07	0.26	-0.17	1.00	
Nonresonant \mathcal{A}_{CP}	-0.02	-0.22	0.03	0.09	0.03	-0.06	0.13	0.27	0.06	1.00

TABLE VI: Comparison of results for the favored and second solutions. The uncertainties are statistical only.

	Favored solution		Second solution	
Inclusive signal yield	1219 \pm 50		1195 \pm 45	
Inclusive signal \mathcal{A}_{CP}	+0.032 \pm 0.044		+0.015 \pm 0.043	
$q\bar{q}$ background yield	2337 \pm 62		2358 \pm 64	
$q\bar{q}$ background \mathcal{A}_{CP}	+0.002 \pm 0.027		+0.011 \pm 0.027	
	Favored solution		Second solution	
Resonance	Fit fraction	\mathcal{A}_{CP}	Fit fraction	\mathcal{A}_{CP}
$\rho^0(770)\pi^\pm$	0.532 \pm 0.037	+0.18 \pm 0.07	0.458 \pm 0.033	+0.03 \pm 0.08
$\rho^0(1450)\pi^\pm$	0.091 \pm 0.023	-0.06 \pm 0.28	0.064 \pm 0.016	-0.54 \pm 0.24
$f_2(1270)\pi^\pm$	0.059 \pm 0.016	+0.41 \pm 0.25	0.079 \pm 0.016	+0.55 \pm 0.20
$f_0(1370)\pi^\pm$	0.189 \pm 0.033	+0.72 \pm 0.15	0.030 \pm 0.019	-1.00 $^{+0.58}_{-0.00}$
Nonresonant	0.349 \pm 0.042	-0.14 \pm 0.14	0.365 \pm 0.042	-0.11 \pm 0.14